Proceedings of 20th International Congress on Acoustics, ICA 2010

23-27 August 2010, Sydney, Australia

Active suppression of acoustic radiation from a submarine hull using inertial actuators

Mauro Caresta and Nicole Kessissoglou

School of Mechanical and Manufacturing Engineering, The University of New South Wales, Sydney NSW 2052, Australia

PACS: 43.40.VN, 43.40.EY, 43.20.TB

ABSTRACT

This work investigates the use of inertial actuators to actively reduce the sound radiated by a submarine hull under harmonic excitation from the propeller. The axial fluctuating forces from the propeller are tonal at the blade passing frequency. The hull is modelled as a fluid loaded cylindrical shell with ring stiffeners and two equally spaced bulkheads. The cylinder is closed by end plates and conical end caps. The forces from the propeller are transmitted to the hull by a rigid foundation connected to the shaft with a thrust bearing. The actuators are arranged in circumferential arrays and attached to the internal end plates of the hull. Two active control techniques corresponding to active vibration control and active structural acoustic control are implemented to attenuate the structural and acoustic responses of the submarine. An acoustic transfer function is defined to estimate the far field sound pressure from a single point measurement on the hull. The inertial actuators are shown to provide control forces with a magnitude large enough to reduce the structure-borne sound due to hull vibration.

INTRODUCTION

Low frequency radiated noise is an important issue in ships and submarines due to the fluctuating forces from the propeller at the blade passing frequency (rotational speed of the shaft multiplied by the number of blades on the propeller). The harmonic forces result from the rotation of the propeller in a spatially non-uniform wake [1]. Due to the size of marine vessels and the magnitude of the forces involved, noise reduction efforts have mainly concentrated on using passive control techniques applied to the propeller-shafting system [2, 3] or modification to the propeller shaft and thrust bearing [4, 5]. A range of passive and active control means have been applied to control the vibration of cylindrical shells, including the use of passive damping layers [6], discrete piezoelectric actuators [7] and an active constrained layer damping treatment [8]. Active control techniques to reduce both the vibration and sound radiated by flexible structures have received much attention in the past three decades. Two main strategies are active vibration control (AVC), which focuses on reducing the vibration level of a structure and active structural acoustic control (ASAC), which aims to reduce structure-borne radiated sound by application of control inputs to the structure [9]. Pan and Hansen [10] present a theoretical analysis of active control of the power transmission in a semi-infinite cylinder using circumferential arrays of control force and error sensors. Maillard and Fuller [11] investigated the use of piezoelectric actuators to reduce the sound radiated by a cylinder using discrete structural acoustic sensing (DSAS), where point sensors on the structure were used to estimate the radiated pressure. Recent work by Pan et al. [12, 13] presents active vibration control of the low frequency hull vibration and radiated noise for a submarine hull, in which the control moment actuation was generated on the radiating hull surface using a stiffener.

In this work, active control techniques are used to reduce the low frequency sound radiated by a submarine hull under axial excitation from the propeller. Inertial actuators are arranged in circumferential arrays and are located on the internal end plates of the hull, in order to produce sufficient secondary forces to reduce the primary effect of the propeller force. The performances of both AVC and DSAS are examined. In the first control strategy, active vibration control is implemented to minimise a cost function based on the structural response. As the use of microphones located in the surrounding fluid medium to directly measure the sound field is not practical for a submarine during operating conditions, discrete structural acoustic sensing (DSAS) has been implemented. Using this control strategy, the far field sound pressure has been estimated using an error sensor located on the structure. The sound radiated by the submarine hull in the far field is described in the frequency domain in terms of the hull axial displacement, in order to define an acoustic transfer function. The transfer function is then used to filter a single measurement point of the axial displacement and estimate the radiated sound pressure at various far field locations. The uncontrolled and controlled structural and acoustic responses of the submarine hull for various arrangements of the two control strategies are presented.

DYNAMIC MODELLING

Submarine hull

The submarine hull is modelled as ring stiffened cylindrical shell with two equally spaced bulkheads and closed at each end by a truncated conical shell. The entire structure is submerged in a heavy fluid medium. A dynamic model of the propeller-shafting system is included in the hull model and consists of the propeller, propeller shaft, thrust bearing and foundation, as shown in Figure 1.

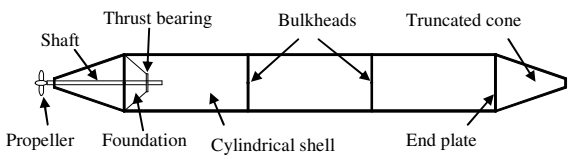

Figure 1. Schematic diagram of a submarine hull

A dynamic model to describe the structural and acoustic responses of the submarine hull shown in Figure 1 under asymmetric excitation has been previously presented by the authors [14]. For completeness of the present study, the model is briefly reviewed here for axisymmetric motion only. A schematic diagram showing the displacements and coordinate system of the coupled cylindrical-conical shell is shown in Figure 2. The cylindrical shell is modelled using the Flügge thin shell theory [15] and the dynamic effect of the ring stiffeners is taken into account by averaging the stiffener properties on the shell [16]. The equations of motion to describe the axisymmetric vibrations of the cylindrical shell are given in terms of *u* and *w*, which correspond to the axial and radial components of the shell displacement as a function of the axial coordinate *x*.

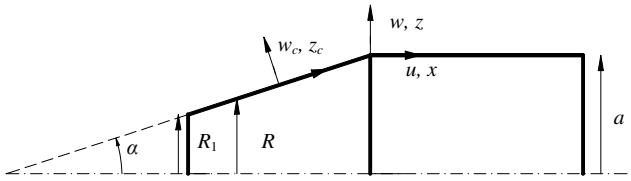

Figure 2. Coupled conical-cylindrical shell

The time harmonic dependence $e^{-j\omega t}$ is omitted in the proceeding analysis. The equations of motion for axisymmetric vibrations of the stiffened fluid loaded shell are given by [14]

$$\frac{\partial^2 u}{\partial x^2}+\frac{\upsilon}{a}\frac{\partial w}{\partial x}-\beta^2 a\frac{\partial^3 w}{\partial x^3}+\frac{\omega^2}{c_L^2}u=0 \tag{1}$$

$$\frac{\upsilon}{a}\frac{\partial u}{\partial x}-\beta^2 a\frac{\partial^3 u}{\partial x^3}+d_1 a^2 w+\beta^2\left(d_2 a^2 w+a^2\frac{\partial^4 w}{\partial x^4}\right) -\frac{\gamma\omega^2}{c_L^2}w-\frac{p}{\rho h c_L^2}=0 \tag{2}$$

$$d_1=1+\frac{A(1-\upsilon^2)}{abh}(a+2z_e)\ ,\ d_2=1+\frac{3EI}{bD}\ ,\ \gamma=1+\frac{A}{bh}+\frac{m_{eq}}{\rho h} \tag{3}$$

ω is the angular frequency. $\beta=h/\sqrt{12}a$ is the thickness parameter, where a and h are the mean radius and thickness of the shell. The ring stiffeners have cross sectional areal *A*, *b* is the stiffener spacing, z_e is the distance between the shell mid-surface and the centroid of a ring, and *I* is the area moment of inertia of the stiffener about its centroid. $D=Eh^3/(12-\upsilon^2)$ is the flexural rigidity and $c_L=[E/\rho(1-\upsilon^2)]^{1/2}$ is the longitudinal wave speed, where *E*, ρ and υ are respectively the Young's modulus, density and Poisson's ratio of the cylinder. m_{eq} is an equivalent distributed mass on the cylindrical shell to take into account the ballast tanks and onboard equipment, which are considered rigidly attached to the shell. The external pressure p can be written in terms of an acoustic impedance Z by [17]

$$p=Z\dot{w}=\frac{j\omega\rho_f H_0[(k_f{}^2-k^2)^{1/2}a]}{(k_f{}^2-k^2)^{1/2}H_0'[(k_f{}^2-k^2)^{1/2}a]}\dot{w} \tag{4}$$

ρ_f is the density of the fluid and *j* is the imaginary unit. k and k_f are respectively the axial and acoustic wave numbers. H_0 is the zero order Hankel function of the first kind and H_0' is its derivative with respect to the argument. The validity of the approximation for the fluid loading in the low frequency range was demonstrated in Ref. [14], in which the structural and acoustic responses of a large submerged vessel were compared with results from a fully coupled finite element/boundary element model. The axial and radial displacements for the cylindrical shell can be written in terms of a wave solution and are respectively given by

$$u(x)=\sum_{i=1}^{6}U_i e^{jk_i x}\ ,\quad w(x)=\sum_{i=1}^{6}W_i e^{jk_i x} \tag{5}$$

where U_i, W_i are respectively the wave amplitude coefficients of the axial and radial displacements.

The equations of motion for a truncated cone of semi-vertex angle α are given in terms of u_c and w_c, which are respectively the orthogonal components of the displacement in the x_c and radial directions, as shown in Figure 2. The equations of motion to describe the axisymmetric dynamic responses of a fluid loaded conical shell are given by [18]

$$\frac{\partial u_c{}^2}{\partial x_c^2}+\frac{\sin\alpha}{R}\frac{\partial u_c}{\partial x_c}-\frac{\sin^2\alpha}{R^2}u_c+\frac{\upsilon\cos\alpha}{R}\frac{\partial w_c}{\partial x_c} -\frac{\sin\alpha\cos\alpha}{R}w_c+\frac{\omega^2}{c_L^2}u_c=0 \tag{6}$$

$$-\frac{\upsilon\cos\alpha}{R}\frac{\partial u_c}{\partial x_c}-\frac{\sin\alpha\cos\alpha}{R^2}u_c-\frac{\cos^2\alpha}{R^2}w_c -\frac{h_c^2}{12}\nabla^4 w_c-\frac{\omega^2}{c_L^2}w_c-\frac{p_c}{\rho h_c c_L^2}=0 \tag{7}$$

where $\nabla^4=\left(\frac{\partial^2}{\partial x_c^2}+\frac{\sin\alpha}{R}\frac{\partial}{\partial x_c}\right)^2$. R is the cone radius at location x_c and h_c is the shell thickness. The external pressure p_c can be written in terms of an acoustic impedance similar to the one used for the cylindrical shell [18]. Expanding the conical shell displacements using a power series and substituting them into the equations of motion results in the following solutions of the form

$$u_c(x_c)=\left[u_{c1}(x_c)\ \ \cdots\ \ u_{c6}(x_c)\right]\cdot\mathbf{x}_c \tag{8}$$

$$w_c(x_c)=\left[w_{c1}(x_c)\ \ \cdots\ \ w_{c6}(x_c)\right]\cdot\mathbf{x}_c \tag{9}$$

$$\mathbf{x}_c=\left[a_0\ \ a_1\ \ c_0\ \ c_1\ \ c_2\ \ c_3\right]^T \tag{10}$$

$u_{ci}(x_c)$ and $w_{ci}(x_c)$ are base functions and $\mathbf{x}_c$ is the unknown coefficients vector. More details on the derivation of the fluid loaded conical shell displacements can be found in Ref. [18]. The cylindrical and conical shell motions are then coupled together by applying the continuity conditions at the junction, as described later in the section Steady State Response.

Propeller-shafting system

The axial thrust force from the propeller is transmitted to the hull by means of the propeller-shafting system that consists of the propeller, shaft, thrust bearing and the foundation. The shaft is idealised as a rod in longitudinal vibration separated in two parts at the connection with the thrust bearing. The thrust bearing is modelled as a single degree of freedom system of mass M_b, stiffness K_b and damping coefficient C_b. The axial force is transmitted to the hull by means of a rigid foundation of conical shape. The propeller is modelled as a lumped mass M_{pr} at the end of the shaft, as shown in Figure 3. The shaft dynamics is described by the displacements u_{s1} and u_{s2} along the x_{s1} and x_{s2} coordinates, respectively. The equation of motion for the free longitudinal vibrations of the shaft and the corresponding steady state solution are given by

$$\frac{\partial^2 u_{si}}{\partial x_{si}^{\ 2}} + \frac{\omega^2}{c_{sL}^2} u_{si} = 0 \tag{11}$$

$$u_{si}(x_{si}) = A_{si} e^{-jk_s x_{si}} + B_{si} e^{jk_s x_{si}}, \qquad i=1,2 \tag{12}$$

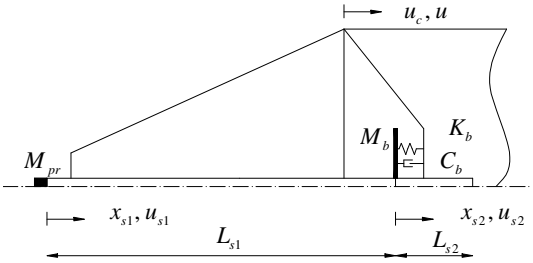

Figure 3. Propeller-shafting system

$k_s = \omega / c_{sL}$ is the axial wavenumber of the shaft, where $c_{sL} = (E_s / \rho_s)^{1/2}$ is the longitudinal wave speed. E_s and ρ_s are the Young's modulus and density of the shaft. The coefficients A_{si} and B_{si} are determined from the boundary conditions, as described in section 4.

Bulkheads

Circular plates are used to model the bulkheads of the cylindrical hull and plates that close each end of the truncated cones. Both in-plane and bending motion of the circular plates is considered. The equations of motion for the axial w_p and radial u_p displacements are given in terms of the radial coordinate *r* by [19]

$$\left(\frac{\partial^2 w_p}{\partial r^2} + \frac{1}{r}\frac{\partial w_p}{\partial r} \right)^2 + \frac{\rho_p h_p \omega^2}{D_p} w_p = 0 \tag{13}$$

$$\frac{\partial}{\partial r}\left(\frac{\partial u_p}{\partial r} + \frac{u_p}{r} \right) + \frac{\omega^2}{c_{pL}^2} u_p = 0 \tag{14}$$

h_p is the plate thickness. $D_p = E_p h_p^3 (12 - \upsilon_p^2)$ is the flexural rigidity and $c_{pL} = [E_p / \rho_p (1 - \upsilon_p^2)]^{1/2}$ is the longitudinal wave speed, where E_p, ρ_p and υ_p are respectively the Young's modulus, density and Poisson's ratio of the circular plate. The solutions for the axial and radial displacements of the circular plate can be expressed in terms of J_0 and I_0 that are respectively the Bessel function and the modified Bessel function of the first kind [19, 20]

$$w_p(r) = A_{p1} J_0(k_{pB} r) + A_{p2} I_0(k_{pB} r) \tag{15}$$

$$u_p(r) = B_{p1} \frac{\partial J_0(k_{pL} r)}{\partial r} \tag{16}$$

$k_{pB} = (\rho_p \omega^2 h_p / D_p)^{1/4}$ is the plate bending wavenumber and $k_{pL} = \omega [\rho_p (1 - \upsilon_p^2) / E_p]^{1/2}$ is the wavenumber for longitudinal in-plane waves. The coefficients A_{p1}, A_{p2} and B_{p1} are determined from the boundary conditions, as described in section 4.

ACTIVE CONTROL

The harmonic excitation from the propeller is at the blade passing frequency (*bpf*). Due to the tonal nature of the primary force, a feedforward active control strategy is appropriate [9]. Two active control strategies are implemented for the reduction of the noise radiated by the submarine, corresponding to active vibration control (AVC) and active structural acoustic control (ASAC), in which discrete structural acoustic sensing (DSAS) is implemented to estimate the radiated pressure using a discrete structural sensor. Using AVC, an error sensor $\mathbf{e}$ at one or more locations on the structure is defined as the sum of the axial displacement $\mathbf{u}_P$ resulting by the primary excitation plus the secondary response $\mathbf{u}_S$ due to the contribution from the secondary forces $\mathbf{f}_S$.

$$\mathbf{e} = \mathbf{u}_P + \mathbf{u}_S, \qquad \mathbf{u}_P = \mathbf{H}_P \mathbf{f}_P, \qquad \mathbf{u}_S = \mathbf{H}_S \mathbf{f}_S \tag{17}$$

$\mathbf{H}_P$ and $\mathbf{H}_S$ are respectively the transfer functions between the primary and secondary forces and the axial displacement. When the number of error sensors exceeds or equates the number of control forces, a cost function to be minimised is defined as [9]

$$J = \mathbf{e}^H \mathbf{e} + \mathbf{f}_S^H \mathbf{R} \mathbf{f}_S \tag{18}$$

The superscript *H* denotes the Hermitian of the vector. $\mathbf{R}$ is a Hermitian positive definite weighting matrix to reduce the values of the control forces to their physical limit and evenly distribute the effort of the actuators. The optimum control force vector is given by [21]

$$\mathbf{f}_{S_o} = -(\mathbf{H}_S^H \mathbf{H}_S + \mathbf{R})^{-1} \mathbf{H}_S^H \mathbf{H}_P \mathbf{f}_P \tag{19}$$

The quadratic optimisation theory described for AVC can also be applied for ASAC, where the goal is to attenuate the structure-borne radiated sound at several locations. An alternative sensing technique to estimate acoustic radiation from structural measurements is implemented here. This technique, known as discrete structural acoustic sensing (DSAS), consists of using arrays of structural sensors whose outputs are filtered to estimate the far field sound pressure with the Helmholtz integral formulation [11, 22, 23]. DSAS provides a practical approach for active control of acoustic signature of maritime vessels. The radiated pressure is calculated by

numerically defining an acoustic transfer function H_{u,p_i} in the frequency domain, that maps the far field sound pressure $p(\theta_i)$ at location θ_i to the displacement $u(x_0)$, as shown in Figure 4, by

$$p(\theta_i) = H_{u,p_i} u(x_0) \tag{20}$$

In this case, the error signal can be written as

$$\mathbf{e} = \mathbf{p}_P + \mathbf{p}_S \tag{21}$$

$$\mathbf{p}_P = \mathbf{H}_{u,p,P}\mathbf{H}_P\mathbf{f}_P \tag{22}$$

$$\mathbf{p}_S = \mathbf{H}_{u,p,S}\mathbf{H}_S\mathbf{f}_S \tag{23}$$

$\mathbf{H}_{u,p,P}$ and $\mathbf{H}_{u,p,S}$ are the matrices containing the acoustic transfer functions due to the primary and secondary forces, respectively.

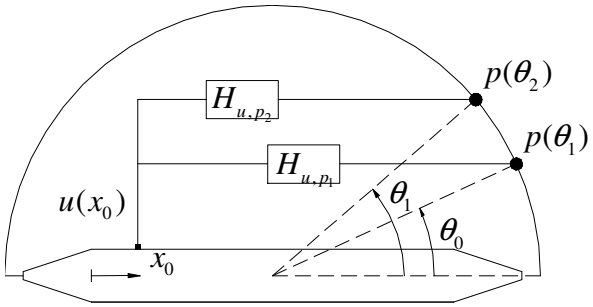

Figure 4. Acoustic transfer function by measurement of the hull structural vibration and radiated sound pressure

Inertial actuators

The secondary forces of the active control application are generated by a circumferential array of inertial actuators attached to the end plates of the cylindrical shell. The inertial actuators have mass m_{ac} and are suspended by a spring of stiffness k_{ac} and damping factor c_{ac}. The electromagnetically generated force f_{ac} acts between the mass and the end plate, as shown in Figure 5.

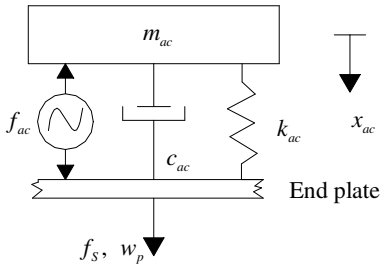

Figure 5. Inertial actuator

The equation of motion for the mass of the inertial actuator is given by

$$m_{ac}\omega^2 x_{ac} = f_{ac} + k_{ac}(x_{ac} - w_p) - j\omega c_{ac}(x_{ac} - w_p) \tag{24}$$

Hence the secondary force f_S transmitted to the plate corresponds to the right hand side of Eq. (24). It is useful to express the transmitted secondary force as a function of the actuator force and plate axial velocity, by rearranging Eq. (24) as

$$f_S = T_{ac} f_{ac} + j\omega Z_{ac} w_p \tag{25}$$

$$T_{ac} = \frac{-\omega^2 m_{ac}}{k_{ac} - \omega^2 m_{ac} - j\omega c_{ac}} \tag{26}$$

$$Z_{ac} = \frac{-j\omega m_{ac} k_{ac} - \omega^2 m_{ac} c_{ac}}{k_{ac} - \omega^2 m_{ac} - j\omega c_{ac}} \tag{27}$$

T_{ac} is the blocked response of the actuator and Z_{ac} is its mechanical impedance. At frequencies higher than the actuator resonance frequency given by $\omega_{ac} = \sqrt{k_{ac}/m_{ac}}$, the blocked response tends to unity and the mass provides a stable inertial platform to react the force [24]. The inertial actuators are positioned on the hull end plate at $r = R_{ac}$ in order to form a circumferential array, as shown in Figure 6. The transmitted force is modelled as a distributed load given by $\frac{f_S}{2\pi R_{ac}}$ where $f_S = \sum_{i=1}^{N} f_{S,i}$. $f_{S,i}$ is a single actuator force and N is the number of actuators.

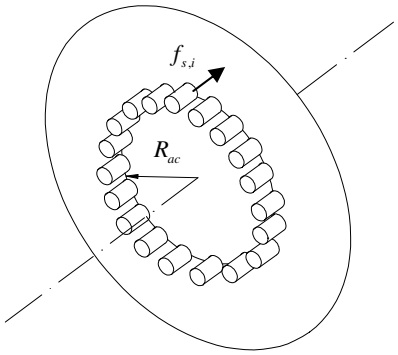

Figure 6. Circumferential actuator array on hull end plate

To dynamically take into account the distributed load due to the circumferential array of inertial actuators, the end plate is modelled as an annular plate enclosing an inner circular plate. The equations of motion for an annular plate in terms of its axial w_a and radial u_a displacements are the same as those for the bulkhead circular plates. However, the solutions for the displacements are now given by [19]

$$\begin{aligned} w_a(r) &= A_{a1}J_0(k_{aB}r) + A_{a2}I_0(k_{aB}r) \\ &+ A_{a3}Y_0(k_{aB}r) + A_{a4}K_0(k_{aB}r) \end{aligned} \tag{28}$$

$$u_a(r) = B_{a1}\frac{\partial J_0(k_{aL}r)}{\partial r} + B_{a2}\frac{\partial Y_0(k_{aL}r)}{\partial r} \tag{29}$$

k_{aB} and k_{aL} are respectively the wavenumbers for the bending and longitudinal in-plane waves. Y_0 and K_0 are respectively the Bessel function and the modified Bessel function of the second kind [20]. The coefficients A_{ai} ($i = 1:4$) and B_{ai} ($i = 1:2$) are determined from the boundary conditions. The circular and the annular plates are joined together by applying continuity of forces, moment, displacements and slope at the junction of the plates. The forces from the inertial actuators are included in the equilibrium of the axial forces. In the

case of two concentric circumferential force arrays applied to the end plate, the plate is modelled as a junction of two annular plates and an inner circular plate.

STEADY STATE RESPONSE

The steady state response of the hull under harmonic force excitation from the propeller and inertial actuators is calculated using a direct method in which the external forces are considered as part of the boundary conditions. The dynamic response of the submarine is expressed in terms of W_i ($i=1:6$) for each section of the hull, A_{pi} ($i=1:2$) and B_{p1} for each full circular plate, A_{ai} ($i=1:4$) and B_{ai} ($i=1:2$) for each annular plate, $\mathbf{x}_c$ for the cone and A_{si}, B_{si} ($i=1:2$) for the shaft. The dynamic response is calculated by assembling the force, moment, displacement and slope continuity conditions at each junction on the hull. The membrane force N_x, bending moment M_x, transverse shearing force Q_x and the Kelvin-Kirchhoff shear force V_x for the shells and plates are given in Ref. [15] per unit length. The slopes are given by $\phi=\partial w/\partial x$ for the cylindrical shell, $\phi_c=\partial w_c/\partial x_c$ for the conical shell, and $\phi_p=\partial w_p/\partial r$, $\phi_a=\partial w_a/\partial r$ for the circular and annular plates, respectively. To take into account the change of curvature between the cylinder and the cone, the following notation was introduced

$$\tilde{u}_c=u_c\cos\alpha-w_c\sin\alpha,\ \tilde{w}_c=w_c\cos\alpha+u_c\sin\alpha \tag{30}$$

$$\tilde{N}_{x,c}=N_{x,c}\cos\alpha-V_{x,c}\sin\alpha,\ \tilde{V}_{x,c}=V_{x,c}\cos\alpha+N_{x,c}\sin\alpha \tag{31}$$

At the junction between the cylinder and cone, the continuity conditions are given by

$$u=\tilde{u}_c=w_a,\ w=\tilde{w}_c=u_a,\ \phi=\phi_c=-\phi_a \tag{32}$$

$$M_x-M_{x,c}+M_{x,a}=0,\ V_x-\tilde{V}_{x,c}-N_{r,a}=0 \tag{33}$$

$$\begin{aligned}&N_x+\tilde{N}_{x,c}-N_{x,a}-(K_b-j\omega C_b)[u_{s1}(x_{s1})-u(x)]=0\\&x_{s1}=L_{s1},\ x=0\end{aligned} \tag{34}$$

Similar continuity conditions can be written at the junction between the cylinder and the bulkheads, as well as between the cone and the small end plates. At the junction between the circular and annular plates ($r=R_{ac}$), the continuity of displacement, slope, force and bending moment are given by

$$w_a(r)=w_p(r),\ u_a(r)=u_p(r),\ \phi_a(r)=\phi_p(r) \tag{35}$$

$$N_{r,a}(r)-N_{r,p}(r)=0,\ M_{x,a}(r)-M_{x,p}(r)=0 \tag{36}$$

$$N_{x,a}(r)-N_{x,p}(r)=\frac{f_S}{2\pi r} \tag{37}$$

In Eq. (37), f_S is the harmonic force from the inertial actuators, as given by Eq. (25). The boundary and continuity conditions for the propeller shaft of cross sectional area A_s are given by

$$E_sA_s\frac{\partial u_{s1}(x_{s1})}{\partial x_{s1}}+\tilde{M}_{pr}\omega^2u_{s1}(x_{s1})=f_P,\qquad x_{s1}=0 \tag{38}$$

$$E_sA_s\frac{\partial u_{s2}(x_{s2})}{\partial x_{s2}}=0,\ x_{s2}=L_{s2} \tag{39}$$

$$\begin{aligned}&E_sA_s\frac{\partial u_{s1}(x_{s1})}{\partial x_{s1}}-E_sA_s\frac{\partial u_{s2}(x_{s2})}{\partial x_{s2}}-(K_b-j\omega C_b)[u_{s1}(x_{s1})-u(x)]=0\\&x_{s1}=L_{s1},\ x_{s2}=0,\ x=0\end{aligned} \tag{40}$$

In Eq. (38), the mass of water M_w displaced by the propeller is added to the propeller mass M_{pr}, resulting in $\tilde{M}_{pr}=M_{pr}+M_w$. The mass load on a propeller of radius a_{pr} is given by $M_w=8/3a_{pr}^3\rho_f$ [25]. f_P is the amplitude of the harmonic force from the propeller. The attachment of the shaft to the power system is considered flexible resulting in the free end boundary condition given by Eq. (39). Equation (40) corresponds to the continuity of axial force at the junction of the propeller shaft with the thrust bearing.

The boundary and continuity equations can be arranged in matrix form $\mathbf{Au}=\mathbf{f}$, where $\mathbf{f}$ is the force vector containing the force f_P from the propeller and f_S from the control actuators. From $\mathbf{u}=\mathbf{A}^{-1}\mathbf{f}$, the unknown coefficients of the various plate and shell displacements can be obtained.

RADIATED SOUND PRESSURE

The sound pressure is given by [26]

$$p(R_r,\theta_r)=\frac{e^{jk_fR_r}}{2R_r}\frac{1}{\omega\rho_fc_f}\int_{z_1}^{z_m}Y(r_0,z_0)e^{-j\alpha_rz_0}\frac{r_0}{\cos\beta_r}dz_0 \tag{41}$$

$$\begin{aligned}Y(r_0,z_0)&=p(r_0,z_0)[\gamma_r\cos\beta_rJ_0'(\gamma_rr_0)+j\alpha_r\sin\beta_rJ_0(\gamma_rr_0)]\\&-\rho_f\omega^2W(r_0,z_0)J_0(\gamma_rr_0)\end{aligned} \tag{42}$$

The surface of the hull is represented by Cartesian coordinates (r,z_r), where z_r is in the axial direction with its origin set at the geometric centre of the hull. a_r is the radius of the structure at location z_r. The surface S_0 extends from z_1 to z_m. (r_0,z_0) is the node location on the hull surface S_0. $\alpha_r=k_f\cos\theta_r$, $\gamma_r=k_f\sin\theta_r$ and $\beta_r=\text{atan}(\partial a_r(z_r)/\partial z_r)$. Once the radial displacement $W(r_0,z_0)$ at each node (r_0,z_0) on the boundary of the structure has been evaluated, the shell surface pressure $p(r_0,z_0)$ at each node on the shell surface can then be calculated by $\mathbf{p}_0=\mathbf{Dw}_0$, where $\mathbf{D}$ is the fluid matrix and $\mathbf{p}_0$, $\mathbf{w}_0$ are the vectors of the surface pressure and radial displacement, respectively [14].

NUMERICAL RESULTS

Numerical results are presented for a submarine hull with a cylindrical shell of radius $a=3.25$ m, thickness $h=0.04$ m, length $L=45$ m and with T-ring stiffeners evenly spaced by $b=0.5$ m. A distributed mass on the shell of $m_{eq}=1500$ kgm^{-2} was used. The hull has two equally spaced bulkheads of thickness $h_p=0.04$. The cylindrical hull is closed by truncated conical end caps with semi-vertex angle of $\alpha=18^\circ$, thickness $h_c=0.014$ m and smaller radius of $R_1=0.50$ m. The thickness of the end plates is the same as for the bulkheads. The propeller has a mass of $M_{pr}=10^4$ kg and radius $a_{pr}=a/2$. The thrust bearing mass, stiffness and damping coefficient are given by $M_b=200$ kg, $K_b=2\times10^{10}$Nm^{-1}

and $C_b = 3\times10^7$ kgs^{-1}. The two sections of the shaft are of length $L_{s1} = 9.0$ m and $L_{s2} = 1.5$ m. All the structures are made of steel with density $\rho = 7800$ kgm^{-3}, Young's modulus $E = 2.1\times10^{11}$ Nm^{-2} and Poisson's ratio $\upsilon = 0.3$. Structural damping was introduced using a complex Young modulus $E(1-j\eta)$, where $\eta = 0.02$ is the structural loss factor.

Results are presented using a harmonic force from the propeller with a unity amplitude and frequency range up to 80 Hz. At maximum speed, a typical *bpf* for a submarine is around 25Hz. Higher values of frequency contain the super harmonics which have a much smaller amplitude [27]. The results can be scaled in the case real data of the excitation is available. Two arrays of actuators are used, in which one actuator array is located on the stern end plate at a circumferential radius of $R_{ac} = 0.5$ m and the other is located on the bow end plate, also at circumferential radius $R_{ac} = 0.5$ m. In each array, 30 inertial actuators are used and are driven in phase. Actuator data from a commercially available model has been used and corresponds to a diameter of $\phi = 90$ mm, suspended mass of $m_{ac} = 2.2$ kg, spring stiffness $k_{ac} = 6130$ Nm^{-1}, damping factor c_{ac} =34.8 kgs^{-1} and a peak force of f_S =45 N. Several control arrangements are examined using the two control strategies, AVC and DSAS. The number and location of the error sensors for each control arrangement is presented in Table 1. For DSAS, the pressure at the far field error locations is estimated by a transfer function with a point measurement on the cylindrical shell at $x = 2$ m. The axial location was chosen away from the bulkhead and end plate junctions to avoid near field vibration.

Table 1. Error sensor locations for various control arrangements

Control Arrangement	Error Sensor Locations
AVC 2*f*, 2*e*	$x = [2, 43]$ m
DSAS 2*f*, 2*e*	$\theta = [0, 180]^\circ$
DSAS 2*f*, 8*e*	$\theta = [0, 15, 30, 75, 105, 150, 165, 180]^\circ$

Figure 8 shows the frequency response function (FRF) at the error sensor location of *x*=2 m along the length of the cylindrical hull. The main hull axial resonances occur at around 22.5 Hz, 43.5 Hz and 70.5 Hz. The small peaks visible at 9.5 Hz and 36 Hz are due to the out-of-plane vibration of the bulkheads and end plates. The resonance of the propeller-shafting system occurs at 48 Hz and is very close to the second axial resonance of the hull. The propeller-shafting system resonance falls in the low frequency range due to the large mass of the propeller which, when summed to the mass of the water displaced by the propeller, becomes around 20 ton ($\tilde{M}_{pr}$ =20 ton). Also shown in Figure 8 is the controlled response of the axial displacement using the third control arrangement, corresponding to DSAS with two control actuator arrays and eight error sensors. The controlled response using AVC results in complete cancellation of the axial displacement and hence is not shown in Figure 8. Using DSAS, significant attenuation of the hull axial resonances occurs. As expected, less attenuation is achieved compared to AVC since the objective of DSAS is to minimise the far field radiated sound pressure.

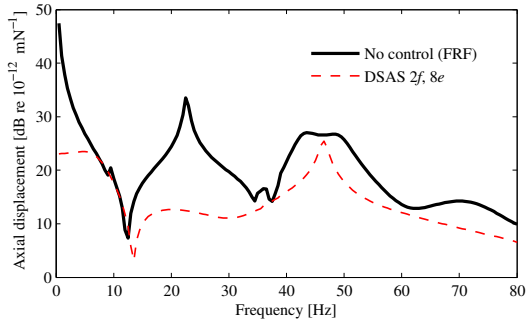

Figure 8. Uncontrolled and controlled responses of the cylindrical hull axial displacement at *x*=2m.

The uncontrolled and controlled sound pressure levels at $\theta = 0$ are shown in Figure 9 using the third control arrangement. A reduction of around 30 dB is observed over almost the entire frequency range. Less attenuation is achieved as the frequency increases and at the propeller-shafting system resonance.

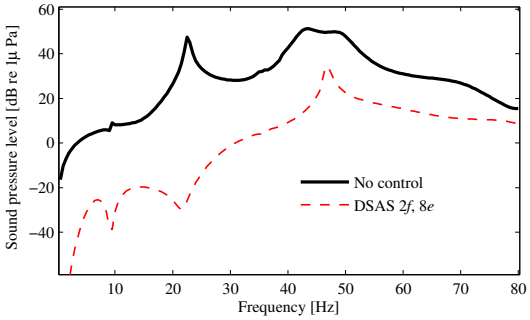

Figure 9. Sound pressure level at $\theta = 0$

Figure 10 presents the uncontrolled and controlled sound power levels using the two DSAS strategies. The controlled responses are similar, although a slight improvement is achieved using eight error sensors compared with a fully determined case (two force arrays and two error sensors). The latter strategy is more attractive due to the reduced complexity in its application. A lack of performance can be observed in the range of 40 to 50 Hz, where two physical system resonances occur in close proximity. Since the actuators are located on the end plates of the hull, the control application can effectively target the hull axial resonances but not the resonance of the propeller-shafting system.

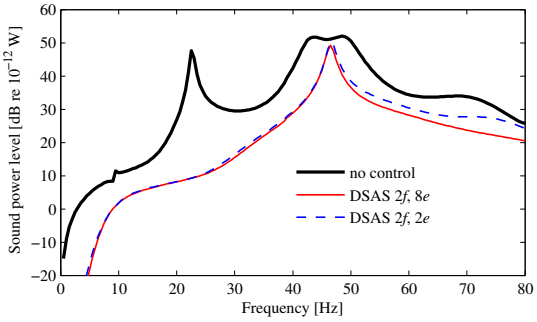

Figure 10 Sound power level.

The uncontrolled and controlled sound power levels using AVC with two control force arrays and two error sensors are shown in Figure 11. Results show that using AVC, a reduction of radiated sound power over the entire frequency range except at the first bulkhead resonance of around 10 Hz, and at

around 45 Hz where the propeller-shafting system and second hull axial resonances occur in close proximity.

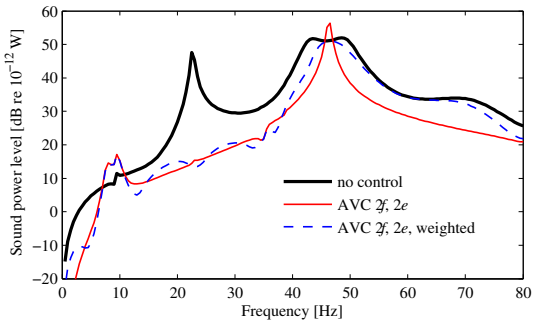

Figure 11 Sound power level.

Figure 12 shows the optimum control forces for AVC (2*f*, 2*e*), the use of a weighting matrix **R** is usefull to distribute the effort of the actuators more equally.

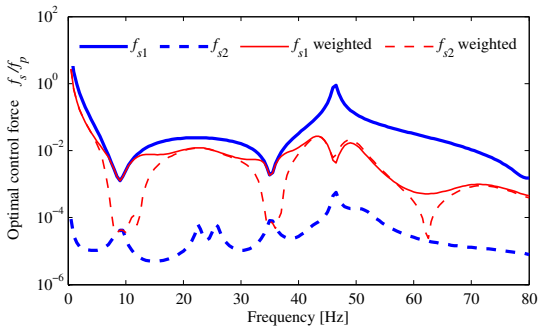

Figure 12 Optimal control force amplitudes of a single actuator in the two control arrays using AVC (2*f*, 2*e*).

Figure 13 presents the ratio of the optimal control force amplitudes to the propeller force for a single inertial actuator in the two control force arrays, using the third control arrangement of DSAS with eight error sensors. To estimate the performances in a real vessel, the propeller force and physical limits of the inertial actuators should be taken into account. A typical blade passing frequency (*bpf*) for a submarine at its maximum speed is around 25 Hz and the amplitude of the fluctuating force is around 2000 N. Using this data, the control force amplitudes for a single actuator in the two control force arrays using DSAS with eight error sensors are $f_{s1} = 34$ N and $f_{s2} = 10.5$ N. These force amplitudes are easily achieved using commercially available inertial actuators. In the frequency range of 40 to 55 Hz, the amplitude of the control forces is significantly higher than at lower frequencies around the fundamental *bpf* of 25 Hz. However, the range above the fundamental *bpf* belongs to the super-harmonics and their amplitudes decrease as the frequency increases.

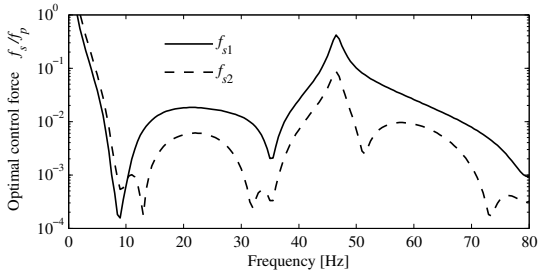

Figure 13 Optimal control force amplitudes of a single actuator in the two control arrays using DSAS (2*f*, 8*e*).

The *bpf* at 25 Hz is very close to the first hull axial resonance at around 22 Hz. The related hull mode has a strong axial component with its ends vibrating out-of-phase to each other. Hence at this frequency, the submarine acts as a woofer and radiates noise with a directivity characteristic associated with an acoustic dipole in the axial direction.

The directivity pattern at the fundamental *bpf* of 25 Hz is shown in Figure 14. Global attenuation of the radiated sound pressure is also observed using AVC or DSAS. The similar levels of attenuation achieved using either control strategy is attributed to the similar levels in attenuation at this frequency in Figs. 11 and 12.

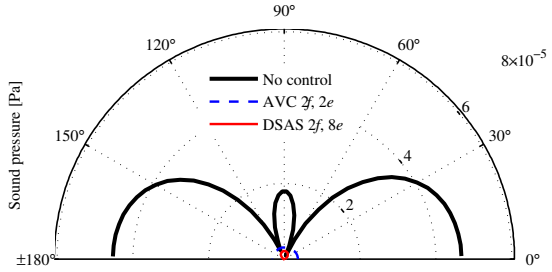

Figure 14 Directivity pattern at the fundamental *bpf* of 25 Hz.

CONCLUSIONS

Two active control strategies corresponding to AVC and DSAS have been used to reduce the sound radiated by a submarine hull under axisymmetric excitation from the propeller. A model of submarine was presented and involved coupling the dynamic responses of cylindrical shells, conical shells and circular plates. A simplified physical model of the propeller-shafting system was also included. An acoustic transfer function was defined in order to estimate the radiated sound by a single point measurement on the hull. The submerged vessel was excited by an axial harmonic force from the propeller. Inertial actuators were located on the end plates of the cylindrical hull and were arranged in circumferential arrays to deliver axisymmetric control forces. It was shown that inertial actuators can deliver sufficient forces to reduce the radiated sound pressure, with very good attenuation over the majority of the frequency range. Future work is required in order to experimentally verify the performance of the active control strategies on a real submerged vessel.

REFERENCES

[1] D. Ross, *Mechanics of underwater sound*, Pergamon, New York, 1976.

[2] A. J. H. Goodwin, "The design of a resonance changer to overcome excessive axial vibration of propeller shafting", *Trans. Inst. Mar. Eng.*, **72**, 37-63 (1960)

[3] P. G. Dylejko, N. J. Kessissoglou, Y. Tso and C. J. Norwood, "Optimisation of a resonance changer to minimise the vibration transmission in marine vessels", *J. Sound Vibrat.*, **300**, 101-116 (2007)

[4] C. P. Rigby, "Longitudinal vibration of marine propeller shafting", *Trans. Inst. Mar. Eng.*, **60**, 67-78 (1948)

[5] H. Schwanecke, "Investigations on the hydrodynamic stiffness and damping of thrust bearings in ships", *Trans. Inst. Mar. Eng.*, **91**, 68-77 (1979)

[6] S. Markus, "Damping properties of layered cylindrical shells vibrating in axially symmetric modes", *Journal of Sound and Vibration*, **48**, 511-524 (1976)

[7] H. C. Lester and S. Lefebvr, "Piezoelectric actuator models for active sound and vibration control of cylinders", *J. Intel. Mat. Syst. Str.*, **4**, 295-306 (1993)

[8] M. C. Ray, J. Oh and A. Baz, "Active constrained layer damping of thin cylindrical shells", *J. Sound Vibrat.*, **240**, 921-935 (2001)

[9] C. R. Fuller, S. J. Elliott and P. A. Nelson, *Active control of vibration*, Academic Press, London, 1996.

[10] X. Pan and C. H. Hansen, "Active control of vibration transmission in a cylindrical shell", *J. Sound Vibrat.*, **203**, 409-434 (1997)

[11] J. P. Maillard and C. R. Fuller, "Active control of sound radiation from cylinders with piezoelectric actuators and structural acoustic sensing", *J. Sound Vibrat.*, **222**, 363-388 (1999)

[12] X. Pan, Y. Tso and R. Juniper, "Active control of radiated pressure of a submarine hull", *J. Sound Vibrat.*, **311**, 224-242 (2008)

[13] X. Pan, Y. Tso and R. Juniper, "Active control of low-frequency hull-radiated noise", *J. Sound Vibrat.*, **313**, 29-45 (2008)

[14] M. Caresta and N. J. Kessissoglou, "Acoustic signature of a submarine hull under harmonic excitation", *Appl. Acoust.*, **71**, 17-31 (2010)

[15] A. W. Leissa, *Vibration of shells*, American Institute of Physics, New York, 1993.

[16] A. Rosen and J. Singer, "Vibrations of axially loaded stiffened cylindrical shells", *J. Sound Vibrat.*, **34**, 357-378 (1974)

[17] M. C. Junger and D. Feit, *Sound, structures, and their interaction*, MIT Press, 2nd, Cambridge, Mass., 1986.

[18] M. Caresta and N. J. Kessissoglou, "Vibration of fluid loaded conical shells", *J. Acoust. Soc. Am.*, **124**, 2068-2077 (2008)

[19] A. W. Leissa, *Vibration of plates*, American Institute of Physics, New York, 1993.

[20] M. Abramowitz and I. A. Stegun, *Handbook of mathematical functions with formulas, graphs, and mathematical tables*, Dover Publications, New York, 1972.

[21] P. A. Nelson and S. J. Elliott, *Active Control of Sound*, Academic Press, London, 1992.

[22] W. T. Baumann, W. R. Saunders and H. H. Robertshaw, "Active suppression of acoustic radiation from impulsively excited structures", *J. Acoust. Soc. Am.*, **90**, 3202-3208 (1991)

[23] J. P. Maillard and C. R. Fuller, "Advanced time domain wave-number sensing for structural acoustic systems. I. Theory and design", *J. Acoust. Soc. Am.*, **95**, 3252-3261 (1994)

[24] L. Benassi, S. J. Elliott and G. P., "Active vibration isolation using an inertial actuator with local force feedback control", *J. Sound Vibrat.*, **276**, 157-179 (2004)

[25] F. J. Fahy, *Sound and Structural Vibration*, Academic Press, London, 1985.

[26] E. A. Skelton and J. H. James, *Theoretical acoustics of underwater structures*, Imperial College Press, London, 1997.

[27] J. P. Breslin and P. Andersen, *Hydrodynamics of ship propellers*, Cambridge University Press, Cambridge, UK, 1994.